

## Article

# Recognition of a Single $\beta$ -D-Xylopyranose Molecule by Xylanase GH11 from *Thermoanaerobacterium saccharolyticum*

Ki Hyun Nam 

College of General Education, Kookmin University, Seoul 02707, Republic of Korea; structure@kookmin.ac.kr

**Abstract:** The endo- $\beta$ -1,4-xylanase glycosyl hydrolase (GH11) decomposes the backbone of xylan into xylooligosaccharides or xylose. These enzymes are important for industrial applications in the production of biofuel, feed, food, and value-added materials.  $\beta$ -D-xylopyranose (XYP, also known as  $\beta$ -D-xylose) is the fundamental unit of the substrate xylan, and understanding its recognition is fundamental for the initial steps of GH11's molecular mechanism. However, little is known about the recognition of a single XYP molecule by GH11. In this study, the crystal structures of GH11 from *Thermoanaerobacterium saccharolyticum* (TsaGH11) complexed with an XYP molecule were determined at a resolution of 1.7–1.9 Å. The XYP molecule binds to subsite –2 of the substrate-binding cleft. The XYP molecule is mainly stabilized by a  $\pi$ - $\pi$  interaction with the conserved Trp36 residue. The O2 and O3 atoms of XYP are stabilized by hydrogen bond interactions with the hydroxyl groups of Tyr96 and Tyr192. The conformation of the thumb domain of TsaGH11 does not play a critical role in XYP binding, and XYP binding induces a shift in the thumb domain of TsaGH11 toward the XYP molecule. A structural comparison of TsaGH11 with other GH11 xylanases revealed that the XYP molecule forms  $\pi$ - $\pi$  stacking with the center between the phenyl and indoline ring of Trp36, whereas the XYP molecule unit from xylobiose or xylotetraose forms  $\pi$ - $\pi$  stacking with the indoline of Trp36, which indicates that the binding modes of the substrate and XYP differ. These structural results provide a greater understanding of the recognition of XYP by the GH11 family.

**Keywords:** xylanase; GH11;  $\beta$ -D-xylopyranose; xylose;  $\beta$ -D-xylose; recognition; *Thermoanaerobacterium saccharolyticum*; crystal structure



**Citation:** Nam, K.H. Recognition of a Single  $\beta$ -D-Xylopyranose Molecule by Xylanase GH11 from

*Thermoanaerobacterium saccharolyticum*. *Crystals* **2024**, *14*, 402. <https://doi.org/10.3390/cryst14050402>

Academic Editor: Borislav Angelov

Received: 16 April 2024

Revised: 24 April 2024

Accepted: 25 April 2024

Published: 26 April 2024



**Copyright:** © 2024 by the author. Licensee MDPI, Basel, Switzerland. This article is an open access article distributed under the terms and conditions of the Creative Commons Attribution (CC BY) license (<https://creativecommons.org/licenses/by/4.0/>).

## 1. Introduction

As industry continues to expand, the demand for fuel is increasing, and the enzymatic conversion of renewable lignocellulosic materials into biofuel is gaining considerable attention as an environmentally friendly and sustainable alternative to fossil fuels [1,2]. Xylan is the major hemicellulose component of plant cell walls and accounts for nearly one-third of the renewable organic carbon sources worldwide [3,4]. Xylan contributes to the rigidity and structural integrity of vascular plants [5]. Xylan consists of a linear D-xylopyranose backbone that is linked by a  $\beta$ -1,4 glycosidic bond, which is branched at the 2- and 3-hydroxy groups with different substituents, such as side-chain substituents, including  $\alpha$ -L-arabinofuranosyl, O-acetyl,  $\alpha$ -1,2-linked glucuronic acid, and 4-O-methyl-D-glucuronic acid groups [6].

Xylanase (EC 3.2.1.8) is the main enzyme for the degradation of xylan and acts on the xylan backbone to cleave the internal site of the  $\beta$ -1,4-glycosidic bond between the xylopyranosyl residues. During this process, xylanase randomly cleaves the xylan backbone and produces a variety of products, such as xylobiose, xylotriose, xylotetraose, and long or branched xylooligomers [7]. In the Carbohydrate-Active enZYme (CAZy) database, glycosyl hydrolase (GH) families 5, 7, 8, 10, 11, 43, and 52 are classified as xylanases [8–10]. Among them, the endo- $\beta$ -1,4-xylanase GH11 performs enzymatic depolymerization of the xylan backbone to generate xylooligosaccharides and xyloses [11] and is considered a “true xylanase” that specifically recognizes xylan [12]. The GH11 xylanase is highly active

on xylan as well as unsubstituted regions of insoluble xylan but has reduced activity on decorated xylan [13].

Xylanase enzymes are widely used in the production of biofuel from agricultural residues, herbaceous crops, forestry residues, wastepaper, and woody crops [14–16]. Moreover, this enzyme is widely applied in industry for pulp bleaching, the deinking of wastepaper, improving the digestibility of animal feed, making bread, producing prebiotics, and producing value-added chemicals [17–19].

The structure of GH11 consists of a single domain within a  $\beta$ -jelly-roll structure with a unique  $\alpha$ -helix packing under  $\beta$ -sheets [12,20]. The typical GH11 substrate-binding site consists of six subsites, namely +3, +2, and +1 to  $-1$ ,  $-2$ , and  $-3$ , where each xylose is anchored through noncovalent interactions [12]. Two catalytic glutamate residues hydrolyze the glycosidic bond that occurs between subsites +1 and  $-1$  [21,22].

To elucidate the molecular mechanism, the crystal structures of GH11 complexed with xylooligomers such as xylotriose and xylobiose have been extensively analyzed [23–26]. However, the identification of a single  $\beta$ -D-xylopyranose (XYP, also known as  $\beta$ -D-xylose) molecule that is the xylan substrate of GH11 remains unknown. The identification thereof is expected to contribute to the understanding of the molecular mechanism for the initial recognition of the first sugar molecule when GH11 recognizes the substrate.

*Thermoanaerobacterium saccharolyticum* is a hemicellulose-degrading thermophilic bacterium [27] that ferments various carbohydrates, including xylan, xylose, glucose, cellobiose, starch, arabinose, mannose, and galactose [28]. *T. saccharolyticum* is utilized as a biological catalyst to convert cellulosic biomass into ethanol [27]. The GH11 from *T. saccharolyticum* (TsaGH11) exhibits a highly efficient  $K_{\text{cat}}$  value of  $34,015 \text{ s}^{-1}$  at pH 5.0 and  $70 \text{ }^\circ\text{C}$  toward beechwood xylan, thus suggesting its attractive potential for industrial applications [29]. To gain a deeper understanding of its enzymatic activity and molecular mechanisms, the room-temperature structure of TsaGH11 was determined using serial synchrotron crystallography and macromolecular crystallography [29–31]. In addition, the crystal structure of TsaGH11 at a basic pH was determined, which revealed subtle pH-induced structural changes of the substrate-binding cleft [32]. This structural information provides insight into the potential industrial application, but the substrate recognition of TsaGH11 remains to be elucidated.

To better understand substrate recognition, the crystal structures of TsaGH11 complexed with XYP were determined at resolutions of 1.7 and 1.9 Å. The XYP molecule was bound to subsite  $-2$  of the substrate-binding cleft and stabilized through  $\pi$ - $\pi$  interactions with the conserved Trp36 residue. XYP induced a positional shift in the thumb domain of TsaGH11. The positioning of XYP at subsite  $-2$  in TsaGH11 was distinct from the XYP unit in the xylooligosaccharides of other GH11 structures. These structural results will expand our understanding of substrate recognition in TsaGH11 as well as the GH11 family.

## 2. Materials and Methods

### 2.1. Protein Preparation

The cloning and purification procedures have been previously reported [29]. Briefly, the recombinant DNA containing the TsaGH11 (UniProt: I3VTR8, 183 residues excluding the signal peptide) gene was transformed into *Escherichia coli* BL21(DE3) competent cells and cultured in Luria–Bertani broth medium with  $50 \text{ } \mu\text{g}/\text{mL}$  kanamycin on an orbital shaker at 180 rpm and  $37 \text{ }^\circ\text{C}$  until reaching an OD600 of 0.6–0.8. Protein expression was induced with  $0.5 \text{ mM}$  isopropyl  $\beta$ -D-1-thiogalactopyranoside (IPTG) and cultured at  $18 \text{ }^\circ\text{C}$  overnight. After cell harvest using centrifugation, the cell pellet was resuspended in lysis buffer containing  $50 \text{ mM}$  Tris-HCl,  $200 \text{ mM}$  NaCl, and  $20 \text{ mM}$  imidazole. The resuspended cells were lysed on ice via sonication. The cell lysate was centrifuged at  $18,894 \times g$  at  $4 \text{ }^\circ\text{C}$  for 1 h. The supernatant was filtered using a  $0.45 \text{ } \mu\text{m}$  syringe filter, and the filtered supernatant was applied to a  $5 \text{ mL}$  Ni-NTA resin column. The resin was washed with  $>10$  column volumes of washing buffer containing  $50 \text{ mM}$  Tris-HCl, pH 8.0,  $300 \text{ mM}$  NaCl, and  $20 \text{ mM}$  imidazole. The proteins were eluted using  $>5$  column volumes

of buffer containing 50 mM Tris-HCl, pH 8.0, 200 mM NaCl, and 300 mM imidazole. The His-tag was cleaved by adding thrombin at room temperature overnight. The sample was concentrated using an Amicon Ultra 15 centrifugal concentrator (10 kDa MWCO) for size-exclusion chromatography. Size-exclusion chromatography was performed using an Akta Start instrument with a HiLoad™ 16/600 Sephacryl S-100 pg column. The purified proteins were then concentrated to 20 mg/mL for crystallization.

## 2.2. Crystallization

The crystallization procedures have been previously reported [32]. Briefly, protein crystallization was performed using the hanging drop vapor diffusion method at 20 °C. The crystallization drop size consisted of 2 µL of the purified TsaGH11 (20 mg/mL) solution and 2 µL of a reservoir containing 0.1 M Tris-HCl, pH 8.5, and 4.0 M ammonium acetate and equilibrated with a reservoir solution (500 µL). Suitable crystals for high-resolution structure determination appeared within 2 months.

## 2.3. X-ray Diffraction Data

X-ray diffraction data were collected at beamline 11C of the Pohang Light Source II (PLS-II, Republic of Korea) using a Pilatus 6M detector [33]. The X-ray wavelength was 0.9794 Å, and the distance between the crystal and detector was 280 mm. The TsaGH11 crystals were soaked in a crystallization solution supplemented with 10 mM XYP for 10 or 30 min. These crystals were further soaked in a cryoprotectant solution containing the crystallization solution supplemented with 20% (*v/v*) glycerol for 10 s. The TsaGH11 crystals were then mounted on the goniometer under a 100 K liquid nitrogen gas stream. The diffraction data were processed with HKL2000 [34].

## 2.4. Structure Determination

The phase problem was solved using molecular replacement using MOLREP [35]. The crystal structure of the apo-state of TsaGH11 at pH 8.5 (PDB code: 8X1D) [32] was used as the search model. Manual model building was performed with COOT [36]. The binding of the XYP molecule was verified through omit map analysis. Structure refinement was performed using the phenix.refine in Phenix [37]. The structure validation was performed using MolProbity [38].

## 2.5. Bioinformatics

Proteins with sequences similar to TsaGH11 were searched using BLAST [39], and amino acid alignment was performed using Clustal Omega [40]. The structure-based multiple sequence alignment was visualized using ESPript 3.0 [41]. The protein structures were visualized with PyMOL (<https://pymol.org/>, accessed on 3 March 2024).

# 3. Results and Discussion

## 3.1. Structure Determination

To better understand the recognition of XYP on TsaGH11, crystal soaking experiments were performed using a crystallization solution containing the XYP molecule. Two sets of diffraction data were collected to identify the reproducibility of the XYP-binding mode. Each TsaGH11 crystal was soaked in the XYP solution for 10 (Data I) or 30 min (Data II). Both TsaGH11-XYP crystals belonged to the tetragonal space group  $P4_32_12$  with similar unit cell dimensions ( $a = b = 73.10$  Å and  $c = 165.10$  Å for Data I, and  $a = b = 73.23$  Å and  $c = 164.78$  Å for Data II) (Table 1). This crystal space group is identical to the previously determined apo-state of TsaGH11 [32], and its unit cell dimensions ( $a = b = 72.79$  Å and  $c = 165.63$  Å) are similar to those of the XYP-bound TsaGH11 structures. The TsaGH11-XYP I and II crystals diffracted to 1.9 Å and 1.7 Å, respectively (Table 1). The final model structures of TsaGH11-XYP I and II were refined using the  $R_{\text{work}}/R_{\text{free}}$  values of 17.21/20.67 and 16.52/19.36, respectively.

**Table 1.** Data collection and refinement statistics of TsaGH11-XYP.

Data Collection	Data I	Data II
X-ray source	Beamline 11C, PLS-II	
Wavelength (Å)	0.9794 Å	
Space group	P4 <sub>3</sub> 2 <sub>1</sub> 2	P4 <sub>3</sub> 2 <sub>1</sub> 2
Cell dimension		
a, b, c (Å)	73.10, 73.10, 165.10	73.23, 73.23, 164.78
α, β, γ (°)	90.00, 90.00, 90.00	90.00, 90.00, 90.00
Resolution (Å)	50.0–1.90 (1.93–1.90)	50.0–1.7 (1.73–1.70)
Unique reflections	35,309 (1721)	49,993 (2406)
Completeness (%)	96.9 (95.7)	99.7 (99.4)
Redundancy	6.0 (4.3)	18.7 (11.6)
I/σ	21.20 (2.04)	9.98 (2.73)
R <sub>merge</sub>	0.109 (0.445)	0.150 (0.552)
CC1/2	0.989 (0.579)	0.996 (0.623)
CC*	0.997 (0.856)	0.999 (0.876)
<b>Refinement</b>		
Resolution (Å)	49.33–1.90	49.40–1.70
R <sub>work</sub> <sup>a</sup>	0.1721	0.1652
R <sub>free</sub> <sup>b</sup>	0.2067	0.1936
RMS deviations		
Bonds (Å)	0.007	0.006
Angles (°)	0.900	0.853
B factors (Å <sup>2</sup> )		
Protein (Chain A/B)	24.59/34.26	16.55/24.22
XYP (Chain A/B)	39.30/41.73	26.34/33.41
Water	40.44	33.32
Ramachandran plot		
Favored (%)	97.51	97.79
Allowed (%)	2.49	2.21
Disallowed (%)	0.00	0.00
PDB code	8YYN	8YYO

Values for the outer shell are given in parentheses. <sup>a</sup>  $R_{\text{work}} = \frac{\sum | |F_{\text{obs}}| - \sum |F_{\text{calc}}| |}{\sum |F_{\text{obs}}|}$ , where  $F_{\text{obs}}$  and  $F_{\text{calc}}$  are the observed and calculated structure-factor amplitudes, respectively. <sup>b</sup>  $R_{\text{free}}$  was calculated as  $R_{\text{work}}$  using a randomly selected subset of unique reflections not used for structural refinement.

The electron density map was observed for the entire amino acid sequence (Thr29–Trp211), excluding the N-terminus. The overall structure of TsaGH11-XYP exhibited a typical β-roll fold resembling a right hand, consisting of finger, palm, and thumb domains (Figure 1A), which indicates that the XYP molecule does not affect the overall structure of TsaGH11. The substrate-binding cleft of TsaGH11 is located between the finger and thumb domains and contains six subsites for xylan substrate binding (Figure 1B). The two TsaGH11 molecules in the asymmetric unit displayed distinct open and closed conformations between the finger and thumb domains (Figure 1C,D). These distinct conformations of TsaGH11 are influenced by the crystal packing effects, which are similar to the previous TsaGH11 structure from the identical tetragonal crystal form [29,32]. In the open conformation of TsaGH11-XYP (Molecule A), the distance between the CH2 atom of Trp36 and the CB atom of Pro143 from Data I and Data II was 5.35 and 5.53 Å, respectively (Figure 1C). In the closed conformation of TsaGH11-XYP (Molecule B), the distance between the CZ2 atom of Trp36 and the CB atom of Pro143 from Data I and Data II was 4.17 and 4.25 Å, respectively (Figure 1D). This indicates that the substrate-binding cleft may be slightly altered depending on the XYP soaking time (see below).

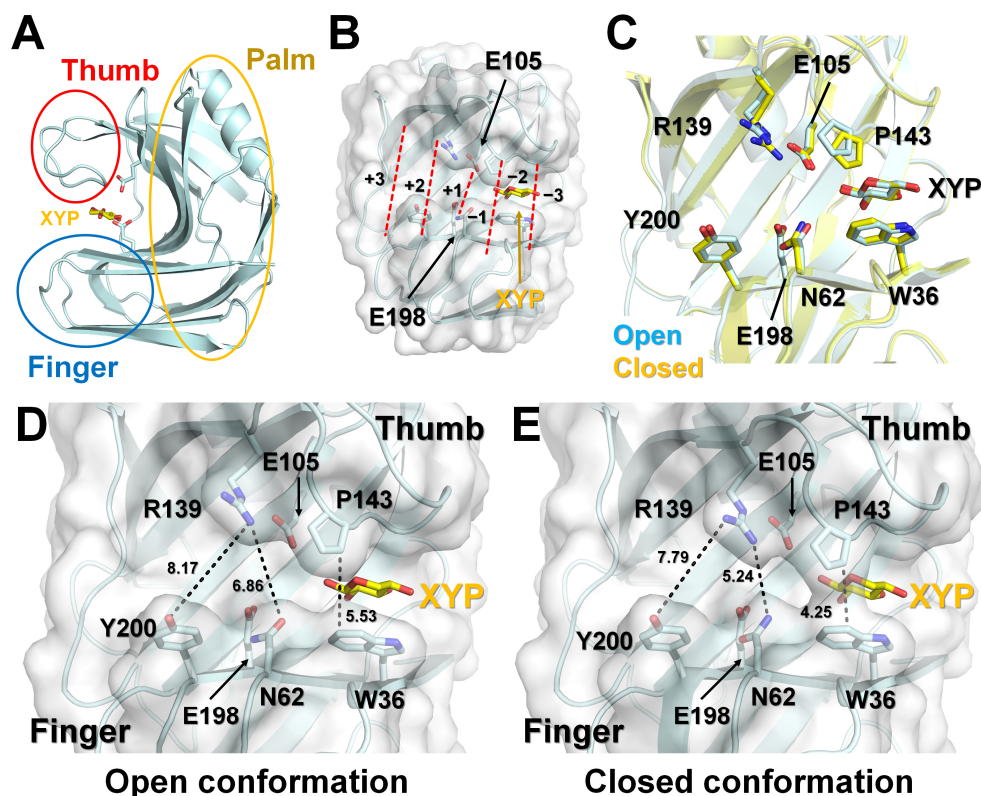


**Figure 1.** Crystal structure of TsaGH11 complexed with XYP. (A) Cartoon representation of the XYP-bound TsaGH11 (Data II, open conformation). Catalytic residues and the XYP molecule are indicated by sticks. (B) Six subsites in the substrate-binding cleft of TsaGH11. (C) Superimposition of the open and closed conformations of TsaGH11-XYP (Data II). Surface structure of the (D) open and (E) closed conformations of TsaGH11-XYP (Data II).

The superimposition of the two TsaGH11 molecules in the asymmetric unit from Data I and II yielded values of 0.200 and 0.170 Å, respectively. The superimposition of each open and closed conformation of TsaGH11-XYP from Data I and II revealed high similarity, with root mean square deviations of 0.070 Å and 0.074 Å, respectively. These results indicate that the open and closed conformations of TsaGH11-XYP from Data I and II are very similar. The B-factor values of the open/closed conformation of TsaGH11-XYP from Data I and II were 24.59/34.26 Å<sup>2</sup> and 16.55/24.22 Å<sup>2</sup>, respectively. These results indicate that the closed conformation of TsaGH11-XYP has relatively higher molecular flexibility because of the exposure to a solvent compared to the rigid conformation of the open conformation of TsaGH11-XYP.

### 3.2. Analysis of XYP Binding in TsaGH11

The positive Fo-Fc electron density map corresponding to the XYP molecule was commonly observed at the −2 subsite of TsaGH11-XYP from Data I and II (Figure 2A), despite TsaGH11 containing six subsites for the binding of XYP units from xylan. This indicates that the −2 subsite of TsaGH11 has a strong affinity for the XYP molecule that constitutes xylan compared to other subsites. This suggests that the −2 subsite of TsaGH11 is crucial for the initial recognition of the xylan substrate.

The B-factor values of XYP in the open/closed conformations of TsaGH11 from Data I and II were 39.30/41.73 Å<sup>2</sup> and 26.34/33.41 Å<sup>2</sup>, respectively, which indicates that the XYP molecule in the open conformation of TsaGH11-XYP was relatively rigid compared to the closed conformation thereof. The XYP molecule is located between Trp36 on the finger domain and the thumb domain. The O1, O2, and O3 atoms of the XYP molecule point toward the palm domain of the substrate-binding cleft of TsaGH11.

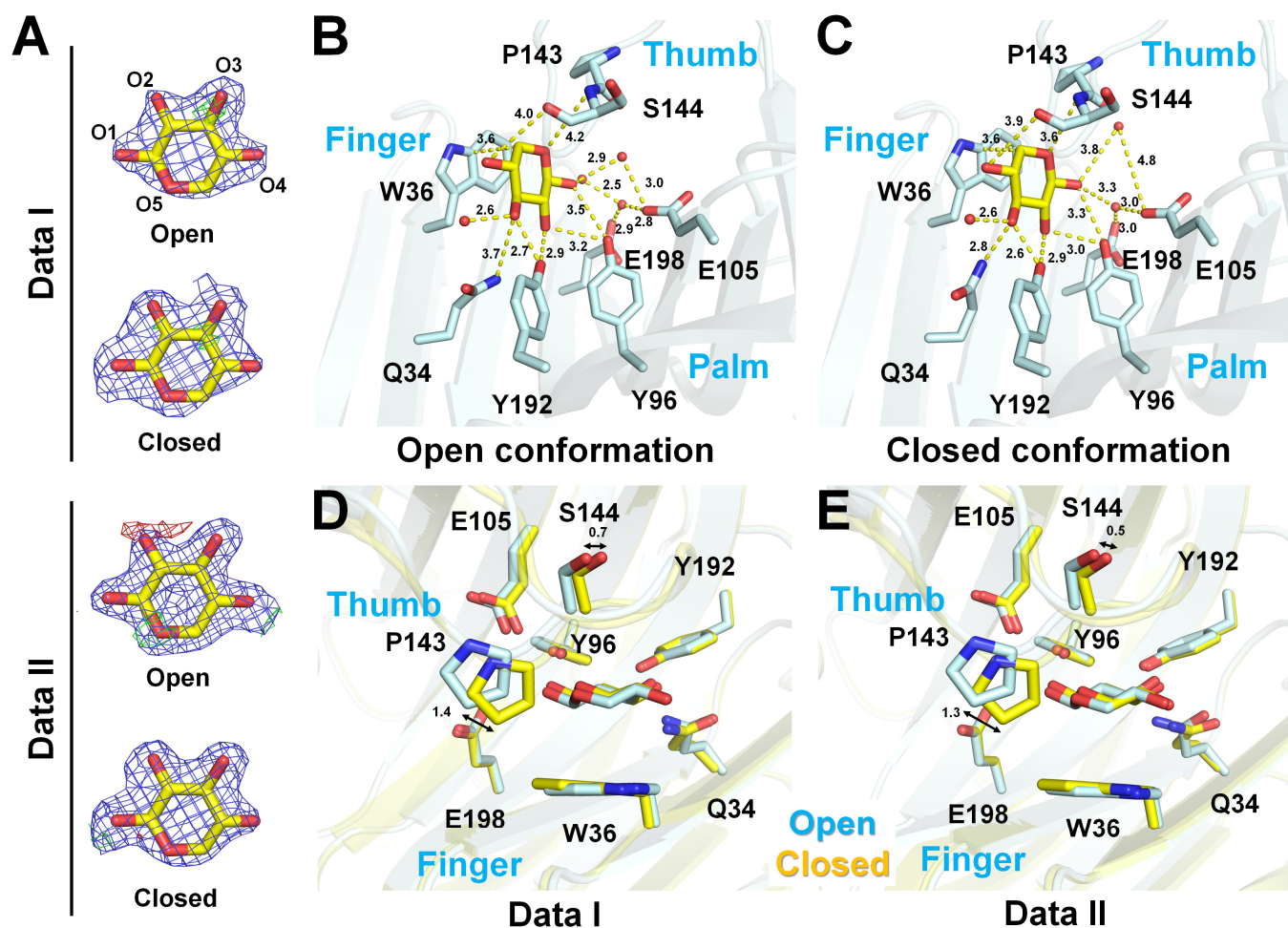


**Figure 2.** XYP binding to the substrate-binding cleft of TsaGH11: (A) 2Fo-Fc electron density maps (1  $\sigma$ , blue mesh) and Fo-Fc electron density maps (+3  $\sigma$ , green mesh;  $-3 \sigma$ , red mesh) of the XYP molecule at the  $-2$  subsite. Interaction between XYP and TsaGH11 in (B) open and (C) closed conformations of TsaGH11-XYP. Superimposition of the open and closed conformations of TsaGH11-XYP from (D) Data I and (E) Data II.

The oxygen atoms of the XYP molecule at the  $-2$  subsite on the substrate-binding cleft interact with the substrate-binding residues (Trp36, Tyr96, Pro143, and Tyr192); however, the interaction distances between the residues and XYP differ depending on the TsaGH11 conformation. In addition, the distance between XYP and TsaGH11 differs slightly depending on the dataset. Here, the interaction between XYP and TsaGH11 is analyzed in detail using the high-resolution Data II of TsaGH11-XYP.

In the open conformation of the substrate-binding cleft of TsaGH11, the O1 atom of XYP interacts with the hydroxyl group of Tyr96 at a distance of 3.46 Å (Figure 2B). The O1 atom of XYP is separated from Glu105 by a distance of 3.99 Å. The O2 atom of XYP interacts with the hydroxyl group of Tyr96 and Tyr192 at distances of 3.17 Å and 2.87 Å, respectively. The O3 atom of XYP interacts with the NE2 atom of Gln34 and the OH atom of Tyr192 at distances of 3.73 and 2.68 Å, respectively. The O4 atom of XYP is separated from the NE1 atom of Trp36 at a distance of 4.02 Å. The O5 atom of XYP is separated from the N atom of Ser144 at a distance of 4.17 Å. The distance between the C5 atom of XYP and the CB atom of Pro143 is 4.92 Å. The distance from the ring center of XYP to the center of Trp36 is 4.04 Å (Figure 2B).

In the closed conformation of the TsaGH11 substrate-binding cleft, the O1 atom of XYP interacts with the hydroxyl group of Tyr96 at a distance of 3.31 Å (Figure 2C). The O1 atom of XYP is separated from Glu105 at a distance of 3.70 Å. The O2 atom of XYP interacts

with the hydroxyl group of Tyr96 and Tyr192 at a distance of 3.02 and 2.92 Å, respectively. The O3 atom of XYP interacts with the NE2 atom of Gln34 and the OH atom of Tyr192 at a distance of 2.82 Å and 2.57 Å, respectively. The O4 atom of XYP is separated from the NE1 atom of Trp36 at a distance of 4.09 Å. The O5 atom of XYP is separated from the N atom of Ser144 at a distance of 3.62 Å. The distance between the C5 atom of XYP and the CB atom of Pro143 is 4.04 Å. The distance from the ring center of XYP to the center of Trp36 is 4.04 Å (Figure 2C).

Taken together, XYP interacts with the amino acids in the finger, palm, and thumb domains of TsaGH11. Among them, Trp36 in the finger domain interacts with XYP at a specific distance because of the  $\pi$ - $\pi$  interaction, regardless of the TsaGH11 conformation. This indicates that Trp36 plays a primary role in the interaction of XYP binding at the -2 subsite, while there are hydrogen bond interactions between the hydroxyl group of Tyr96 and Tyr192 in the palm domain, and the oxygen atoms of XYP determine the orientation of XYP within the substrate-binding site of TsaGH11.

Conversely, in the +2 subsite of TsaGH11-XYP in Data II, a long electron density map was observed (Supplementary Figure S1), which was not observed in TsaGH11-Apo and TsaGH11-XYP in Data I. In the 2Fo-Fc electron density map at the 0.7 $\sigma$  contour level, an electron density map corresponding to XYP was observed. As a result of modeling the XYP molecule, the ring structure of XYP and part of the hydroxyl group fit appropriately with the electron density map (Supplementary Figure S1). However, the XYP molecules were not observed at contour level 1 $\sigma$  of the electron density map; therefore, the XYP molecule was not built into the final model structure. This electron density map tentatively indicates that the XYP molecule can also bind to the +2 subsite in addition to the -2 subsite of TsaGH11. However, considering the substrate concentration and incubation time used during the soaking experiment, the affinity or specificity for the single XYP binding at the +2 subsite position is considered to be very low.

However, after hydrolysis of the xylan substrate by TsaGH11, XYP molecules could be generated as reaction products. This indicates that when a high concentration of reaction products is present with TsaGH11 for an extended period, XYP molecules could bind to the -2 and +2 subsites of TsaGH11, which could act as an inhibitor.

### 3.3. Structure Comparison of Apo and XYP Binding in TsaGH11

To elucidate the structural changes in the substrate-binding cleft because of XYP binding, the open and closed conformations of the high-resolution TsaGH11-XYP (Data II) and TsaGH11-Apo (PDB code: 8X1D) structures were compared. The superimposition of the open and closed conformations of TsaGH11-XYP and TsaGH11-Apo resulted in a root mean square deviation (RMSD) of 0.081 Å and 0.091 Å, respectively.

In the superimposed open conformations of the TsaGH11-XYP and TsaGH11-Apo structures, a substantial shift in the position of the thumb domain was observed (Figure 3A). Specifically, the thumb domain of TsaGH11-XYP moved closer to the -2 subsite of the substrate-binding cleft compared to that of TsaGH11-Apo. In the open conformation of TsaGH11-XYP, the main chains of the Pro143 and Ile145 residues on the thumb domain shifted toward the -2 subsite of the substrate-binding cleft by approximately 0.61 Å and 0.66 Å, respectively, compared to that of TsaGH11-Apo. These results suggest that the XYP molecule induces a positional shift of the thumb domain toward the XYP binding site, which indicates that the thumb domain also contributes to stabilizing the XYP molecule.

In the open conformation, the CE2 atoms of Trp36 in TsaGH11-XPS and TsaGH11-Apo were separated from the CE2 atom of Trp98 by a distance of 9.53 and 9.29 Å, respectively (Figure 3A). The CH2 atoms of Trp36 in TsaGH11-XPS and TsaGH11-Apo were separated from the CB atom of Pro143 on the thumb domain by a distance of 5.53 Å and 5.84 Å, respectively (Figure 3A). This indicates that upon XYP binding in the open conformation of TsaGH11, the width of the substrate-binding cleft of the -2 subsite increases.

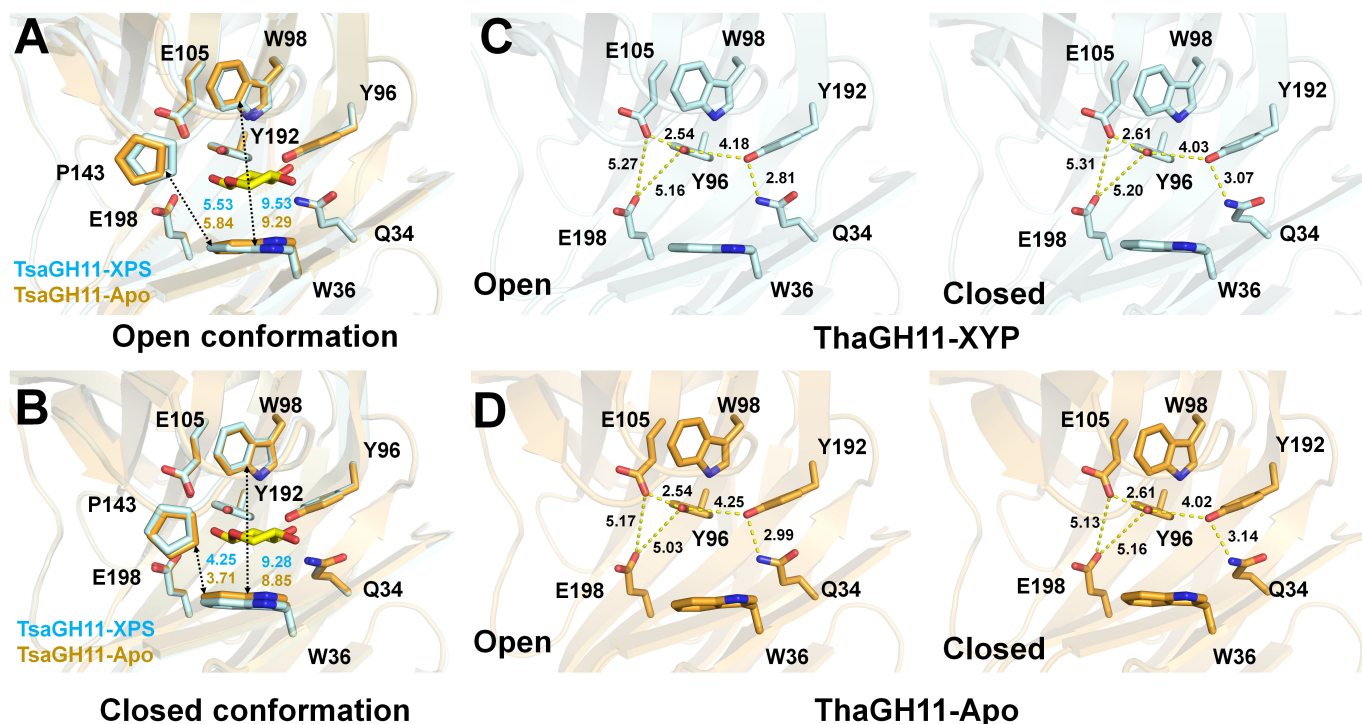


**Figure 3.** Structural comparison of TsaGH11-XYP and TsaGH11-Apo. Superimposition of the (A) open and (B) closed conformations of TsaGH11-XYP (cyan) and TsaGH11-Apo (orange). Analysis of the catalytic residues and conserved Tyr96 and Tyr192 residue interactions on the palm domain for the open and closed conformations of (C) TsaGH11-XYP and (D) TsaGH11-Apo.

In the closed conformation, the CE2 atoms of Trp36 in TsaGH11-XPS and TsaGH11-Apo were separated from the CE2 atom of Trp98 by a distance of 9.28 and 8.85 Å, respectively (Figure 3B). The CH2 atoms of Trp36 in TsaGH11-XPS and TsaGH11-Apo were separated from the CB atom of Pro143 in the thumb domain by a distance of 3.71 Å and 4.25 Å, respectively (Figure 3B). This indicates that in the closed form of TsaGH11 when XYP binds, the width of the substrate-binding cleft of the −2 subsite increases, and the thumb region, which was close to the finger domain in TsaGH11-Apo, moves away from the XYP molecule. As a result, the binding of XYP has structural effects around the −2 subsite and thumb domain of TsaGH11.

Next, the structural effects of the catalytic and conserved Tyr residues in the palm domain because of XYP binding were investigated. A substantial change occurred in the distance between the Glu105 and Glu198 catalytic residues of the active site between TsaGH11-XYP and TsaGH11-Apo (Figure 3C,D). The distances between the catalytic residues in the open/closed conformation of TsaGH11-XYP and TsaGH11-Apo were 5.27/5.31 and 5.17/5.13 Å, respectively. This indicates that when XYP binds to the −2 subsite, the width of the substrate-binding cleft at the active site region expands, which may provide sufficient space and allow the substrate access to the −1 and +1 subsites.

Regarding the conserved Tyr residues in the palm domain of the TsaGH11-XYP open conformation, the hydroxyl group of Tyr96 interacted with the OE2 atom of Glu105 and the OE1 atom of Glu198 at a distance of 2.54 Å and 5.16 Å, respectively. The hydroxyl group of Tyr192 interacted with the NE1 atom of Gln34 and the hydroxyl group of Tyr96 at a distance of 2.81 Å and 4.18 Å, respectively (Figure 3C). In the TsaGH11-XYP closed conformation, the hydroxyl group of Tyr96 interacted with the OE2 atom of Glu105 and the OE1 atom of Glu198 at a distance of 2.61 Å and 5.20 Å, respectively. The hydroxyl group of Tyr192 interacted with the NE1 atom of Gln34 and the hydroxyl group of Tyr96 at a distance of 3.07 Å and 4.03 Å, respectively (Figure 3C).

In the TsaGH11-Apo open conformation, the hydroxyl group of Tyr96 interacted with the OE2 atom of Glu105 and the OE1 atom of Glu198 at a distance of 2.54 Å and 5.03 Å, respectively (Figure 3D). The hydroxyl group of Tyr192 interacted with the NE1 atom of Gln34 and the hydroxyl group of Tyr96 at a distance of 2.99 Å and 4.25 Å, respectively (Figure 3D). In the TsaGH11-Apo closed conformation, the hydroxyl group of Tyr96 interacted with the OE2 atom of Glu105 and the OE1 atom of Glu198 at a distance of 2.61 Å and 5.16 Å, respectively. The hydroxyl group of Tyr192 interacted with the NE1 atom of Gln34 and the hydroxyl group of Tyr96 at a distance of 3.14 Å and 4.02 Å, respectively (Figure 3D).

Taken together, no significant structural differences were observed in the interaction of Tyr96 and Tyr192 in the palm domain with the surrounding amino acids when TsaGH11-XYP and TsaGH11-Apo were in the same conformation. However, a structural difference between the conserved Tyr96 and Tyr192 in the palm domain was observed when TsaGH11 was in a different conformation than when XYP was bound to TsaGH11. This indicates that the conformation of TsaGH11 affects the positional arrangement of the conserved amino acids within the palm domain.

### 3.4. Structure Comparison of TsaGH11-XYP with Other GH11s

To understand the structural similarities and differences between the recognition of a single XYP molecule and oligoxylose by GH11, the crystal structures of TsaGH11-XYP and oligoxylose-bound GH11 were compared. Through the BLAST analysis, among the GH11s with amino acid sequences similar to TsaGH11, the reported protein crystal structures included XynA from *Bacillus subtilis* (BsXynA, UniProt: P18429, sequence identity: 72.8%), XynA from *Niallia circulans* (NciXynA, P09850, 72.8%), GH11 from *Paenibacillus xylanivorans* (PxyGH11, A0A0M9BNX9, 69.6%), and Xyn11A from *Thermopolyspora flexuosa* (TfxXyn11A, Q8GMV7, 56.8%) (Figure 4A and Supplementary Figure S2). Among these, BsXynA (PDB code: 2QZ3) and NciXynA (1BCX) were mutated to Glu172Ala and Glu172Cys, respectively, and their structures were determined in complex with xylotriose (XYP3) and xylobiose (XYP2), respectively. In BsXynA-XYP3, the XYP molecules were located at the −1, −2, and −3 subsites (Figure 4B). In NciXynA-XYP2, the XYP molecules were located at the −1 and −2 subsites (Figure 4C). The position of the XYP molecules at the −1 and −2 subsites in BsXynA-XYP3 and NciXynA-XYP2 was similar within a subtle movement of <0.6 Å (Supplementary Figure S3). The superimposition of the open/closed conformations of TsaGH11-XYP compared with BsXynA-XYP4 and NciXynA-XYP2 revealed structural similarity with an RMSD of 0.363/0.324 Å (average of two molecules in the asymmetric unit) and 0.275/0.246 Å, respectively. However, the position of the XYP molecule in TsaGH11 was distinct, with the XYP unit at the −2 subsite in BsXynA-XYP3 and NciXynA-XYP2 (Figure 4B,C). The XYP molecule at the −2 subsite in TsaGH11 was shifted by approximately 1.2 Å toward the catalytic residue direction when compared with that of BsXynA-XYP3 and NciXynA-XYP2. In a plan view based on Trp36, the center of the XYP ring bound to TsaGH11 lies at the center of the indole and phenol rings of Trp36 (Figure 4D). Meanwhile, the XYP molecule at the −2 subsite in BsXynA-XYP3 and NciXynA-XYP2 lies in the center of the indole ring of Trp36 (Figure 4D). These results indicate that the recognition and binding modes of a single XYP and oligoxylose molecule by GH11 differ at the −2 subsite. These results indicate that if the XYP unit of the xylan substrate first recognizes and binds at the −2 subsite of TsaGH11, and then other XYP units from xylan bind to another subsite (e.g., the −1 subsite), the XYP molecule that first bound to the −2 subsite may undergo positional rearrangement.

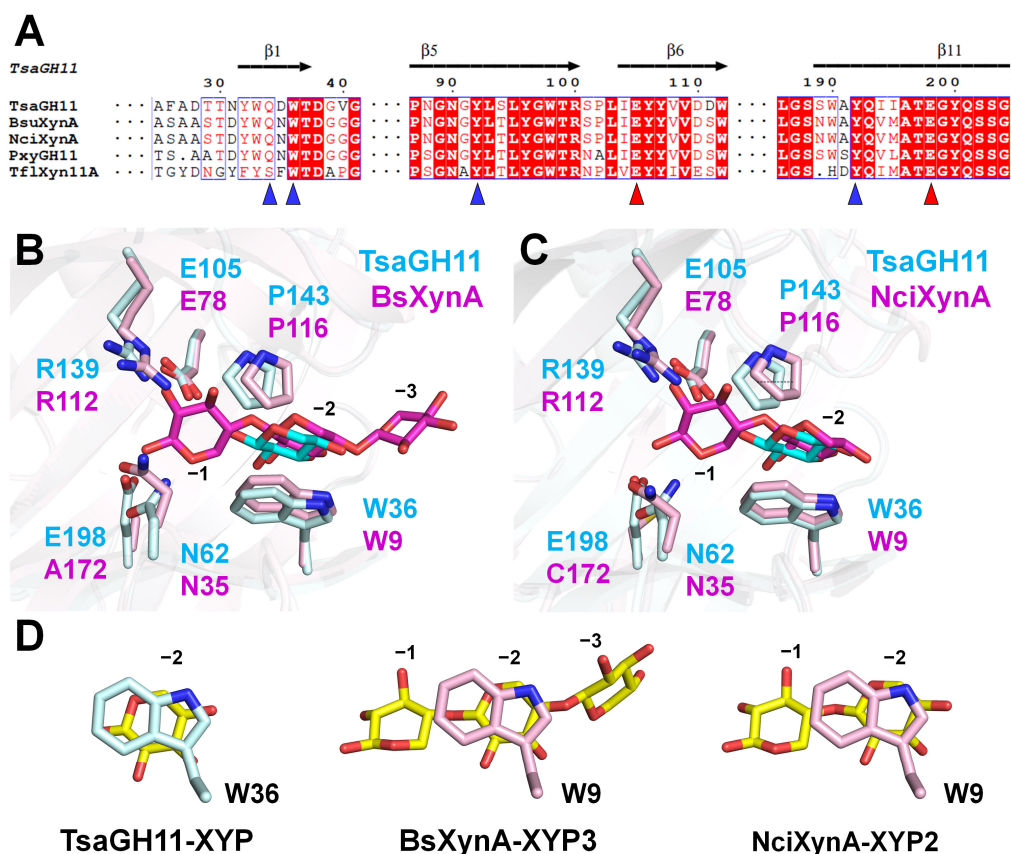


**Figure 4.** Amino acids and structural comparison of TsaGH11-XYP with other GH11 family proteins. (A) Partial multiple sequence alignment of TsaGH11 (UniProt: I3VTR8) with BsXynA (P18429), NciXynA (P09850), PxyGH11 (A0A0M9BNX9), and TflXyn11A (Q8GMV7). The catalytic and XYP-binding residues in TsaGH11-XYP are indicated by red and blue triangles, respectively. Superimposition of TsaGH11-XYP (cyan) compared with (B) BsXynA-XYP3 (PDB code: 2QZ3, pink) and (C) NciXyn-XYP2 (1BCX, pink). (D) Interaction between XYP molecule and Trp residues from TsaGH11-XYP, BsXynA-XYP3, and NciXyn-XYP2.

Alternatively, Qln34 of TsaGH11 is not conserved among the GH11 family (Figure 4A). For example, Qln34 in TsaGH11 is replaced by a Ser residue in TflXyn11A (Figure 4A and Supplementary Figure S3). These results indicate that the binding configuration of the XYP molecule in TsaGH11 may differ among the GH11 proteins with different amino acid sequences that interact with the XYP molecule. In addition, differences in the XYP molecule interacting amino acids are considered to affect the initial substrate recognition and binding of GH11, which results in differences in the reaction rate and cleavage efficiency.

#### 4. Conclusions

Structural information on substrate recognition by GH11 is critical not only for understanding their mechanism of action but also for providing insight into protein engineering for the efficient application of GH11. In this study, the structure for the recognition of a single XYP molecule, a component of the xylan substrate, is reported for the first time. These structural analyses will expand the knowledge on XYP recognition and the structural changes of TsaGH11, as well as substrate recognition by the GH11 family.

**Supplementary Materials:** The following supporting information can be downloaded at <https://www.mdpi.com/article/10.3390/cryst14050402/s1>, Figure S1: Electron density maps of TsaGH11-XYP; Figure S2: Structure-based multiple sequence alignment of TsaGH11 compared with other xylanase; Figure S3: Superimposition of BsXynA-XYP3 and NciXyn-XYP2; Table S1: Interaction between TsaGH11 and the XYP molecule.

**Funding:** This work was funded by the National Research Foundation of Korea (NRF) (NRF-2021R111A1A01050838).

**Data Availability Statement:** Coordinates and structure-factor amplitudes for both structures have been deposited in the PDB under the accession codes 8YYN (Data I) and 8YYO (Data II).

**Acknowledgments:** I would like to thank the beamline staff at the 11C beamline at the Pohang Accelerator Laboratory for their assistance with data collection.

**Conflicts of Interest:** The author declares no conflicts of interest.

## References

1. Srivastava, N.; Rawat, R.; Singh Oberoi, H.; Ramteke, P.W. A Review on Fuel Ethanol Production from Lignocellulosic Biomass. *Int. J. Green Energy* **2014**, *12*, 949–960. [[CrossRef](#)]
2. Srivastava, N.; Srivastava, M.; Mishra, P.K.; Gupta, V.K.; Molina, G.; Rodriguez-Couto, S.; Manikanta, A.; Ramteke, P.W. Applications of fungal cellulases in biofuel production: Advances and limitations. *Renew. Sustain. Energy Rev.* **2018**, *82*, 2379–2386. [[CrossRef](#)]
3. Scheller, H.V.; Ulvskov, P. Hemicelluloses. *Annu. Rev. Plant Biol.* **2010**, *61*, 263–289. [[CrossRef](#)]
4. Collins, T.; Gerday, C.; Feller, G. Xylanases, xylanase families and extremophilic xylanases. *FEMS Microbiol. Rev.* **2005**, *29*, 3–23. [[CrossRef](#)]
5. Martínez-Abad, A.; Berglund, J.; Toriz, G.; Gatenholm, P.; Henriksson, G.; Lindström, M.; Wohlert, J.; Vilaplana, F. Regular Motifs in Xylan Modulate Molecular Flexibility and Interactions with Cellulose Surfaces. *Plant Physiol.* **2017**, *175*, 1579–1592. [[CrossRef](#)]
6. Rennie, E.A.; Scheller, H.V. Xylan biosynthesis. *Curr. Opin. Biotechnol.* **2014**, *26*, 100–107. [[CrossRef](#)]
7. Malgas, S.; Mafa, M.S.; Mkabayi, L.; Pletschke, B.I. A mini review of xylanolytic enzymes with regards to their synergistic interactions during hetero-xylan degradation. *World J. Microbiol. Biotechnol.* **2019**, *35*, 187. [[CrossRef](#)]
8. Henrissat, B. A classification of glycosyl hydrolases based on amino acid sequence similarities. *Biochem. J.* **1991**, *280*, 309–316. [[CrossRef](#)]
9. Marasinghe, S.D.; Jo, E.; Hettiarachchi, S.A.; Lee, Y.; Eom, T.-Y.; Gang, Y.; Kang, Y.-H.; Oh, C. Characterization of glycoside hydrolase family 11 xylanase from *Streptomyces* sp. strain J103; its synergetic effect with acetyl xylan esterase and enhancement of enzymatic hydrolysis of lignocellulosic biomass. *Microb. Cell Fact.* **2021**, *20*, 129. [[CrossRef](#)]
10. Cantarel, B.L.; Coutinho, P.M.; Rancurel, C.; Bernard, T.; Lombard, V.; Henrissat, B. The Carbohydrate-Active EnZymes database (CAZy): An expert resource for Glycogenomics. *Nucleic Acids Res.* **2009**, *37*, D233–D238. [[CrossRef](#)]
11. Chakdar, H.; Kumar, M.; Pandiyan, K.; Singh, A.; Nanjappan, K.; Kashyap, P.L.; Srivastava, A.K. Bacterial xylanases: Biology to biotechnology. *3 Biotech* **2016**, *6*, 150. [[CrossRef](#)] [[PubMed](#)]
12. Paës, G.; Berrin, J.-G.; Beaugrand, J. GH11 xylanases: Structure/function/properties relationships and applications. *Biotechnol. Adv.* **2012**, *30*, 564–592. [[CrossRef](#)]
13. Mendis, M.; Simsek, S. Production of structurally diverse wheat arabinoxylan hydrolyzates using combinations of xylanase and arabinofuranosidase. *Carbohydr. Polym.* **2015**, *132*, 452–459. [[CrossRef](#)] [[PubMed](#)]
14. Uday, U.S.P.; Choudhury, P.; Bandyopadhyay, T.K.; Bhunia, B. Classification, mode of action and production strategy of xylanase and its application for biofuel production from water hyacinth. *Int. J. Biol. Macromol.* **2016**, *82*, 1041–1054. [[CrossRef](#)] [[PubMed](#)]
15. Chaudhary, R.; Kuthiala, T.; Singh, G.; Rarotra, S.; Kaur, A.; Arya, S.K.; Kumar, P. Current status of xylanase for biofuel production: A review on classification and characterization. *Biomass Convers. Biorefin.* **2021**, *13*, 8773–8791. [[CrossRef](#)]
16. Dodd, D.; Cann, I.K.O. Enzymatic deconstruction of xylan for biofuel production. *GCB Bioenergy* **2009**, *1*, 2–17. [[CrossRef](#)]
17. Kim, I.J.; Kim, S.R.; Bornscheuer, U.T.; Nam, K.H. Engineering of GH11 Xylanases for Optimal pH Shifting for Industrial Applications. *Catalysts* **2023**, *13*, 1405. [[CrossRef](#)]
18. Ravn, J.L.; Thøgersen, J.C.; Eklöf, J.; Pettersson, D.; Ducatelle, R.; van Immerseel, F.; Pedersen, N.R. GH11 xylanase increases prebiotic oligosaccharides from wheat bran favouring butyrate-producing bacteria in vitro. *Anim. Feed Sci. Technol.* **2017**, *226*, 113–123. [[CrossRef](#)]
19. Walia, A.; Guleria, S.; Mehta, P.; Chauhan, A.; Parkash, J. Microbial xylanases and their industrial application in pulp and paper biobleaching: A review. *3 Biotech* **2017**, *7*, 11. [[CrossRef](#)]
20. Törrönen, A.; Harkki, A.; Rouvinen, J. Three-dimensional structure of endo-1,4-beta-xylanase II from *Trichoderma reesei*: Two conformational states in the active site. *EMBO J.* **1994**, *13*, 2493–2501. [[CrossRef](#)]
21. Quiocho, F.A. Molecular Features and Basic Understanding of Protein-Carbohydrate Interactions: The Arabinose-Binding Protein-Sugar Complex. In *Carbohydrate-Protein Interaction*; Springer: Berlin/Heidelberg, Germany, 1988; pp. 135–148.
22. Davies, G.J.; Wilson, K.S.; Henrissat, B. Nomenclature for sugar-binding subsites in glycosyl hydrolases. *Biochem. J.* **1997**, *321*, 557–559. [[CrossRef](#)] [[PubMed](#)]
23. Sabini, E.; Sulzenbacher, G.; Dauter, M.; Dauter, Z.; Jørgensen, P.L.; Schüle, M.; Dupont, C.; Davies, G.J.; Wilson, K.S. Catalysis and specificity in enzymatic glycoside hydrolysis: A 2,5B conformation for the glycosyl-enzyme intermediate revealed by the structure of the *Bacillus agaradhaerens* family 11 xylanase. *Chem. Biol.* **1999**, *6*, 483–492. [[CrossRef](#)] [[PubMed](#)]

24. Li, Z.; Zhang, X.; Li, C.; Kovalevsky, A.; Wan, Q. Studying the Role of a Single Mutation of a Family 11 Glycoside Hydrolase Using High-Resolution X-ray Crystallography. *Protein J.* **2020**, *39*, 671–680. [[CrossRef](#)]
25. Cheng, Y.-S.; Chen, C.-C.; Huang, C.-H.; Ko, T.-P.; Luo, W.; Huang, J.-W.; Liu, J.-R.; Guo, R.-T. Structural Analysis of a Glycoside Hydrolase Family 11 Xylanase from *Neocallimastix patriciarum*. *J. Biol. Chem.* **2014**, *289*, 11020–11028. [[CrossRef](#)]
26. Wan, Q.; Zhang, Q.; Hamilton-Brehm, S.; Weiss, K.; Mustyakimov, M.; Coates, L.; Langan, P.; Graham, D.; Kovalevsky, A. X-ray crystallographic studies of family 11 xylanase Michaelis and product complexes: Implications for the catalytic mechanism. *Acta Crystallogr. D Biol.* **2013**, *70*, 11–23. [[CrossRef](#)]
27. Shaw, A.J.; Podkaminer, K.K.; Desai, S.G.; Bardsley, J.S.; Rogers, S.R.; Thorne, P.G.; Hogsett, D.A.; Lynd, L.R. Metabolic engineering of a thermophilic bacterium to produce ethanol at high yield. *Proc. Natl. Acad. Sci. USA* **2008**, *105*, 13769–13774. [[CrossRef](#)] [[PubMed](#)]
28. Lee, Y.E.; Jain, M.K.; Lee, C.Y.; Lowe, S.E.; Zeikus, J.G. Taxonomic Distinction of Saccharolytic Thermophilic Anaerobes: Description of *Thermoanaerobacterium xylanolyticum* gen. nov., sp. nov., and *Thermoanaerobacterium saccharolyticum* gen. nov., sp. nov.; Reclassification of *Thermoanaerobium Brockii*, *Clostridium thermosulfurogenes*, and *Clostridium thermohydrosulfuricum* E100-69 as *Thermoanaerobacter Brockii* comb. nov., *Thermoanaerobacterium thermosulfurigenes* comb. nov., and *Thermoanaerobacter thermohydrosulfuricus* comb. nov., Respectively; and Transfer of *Clostridium thermohydrosulfuricum* 39E to *Thermoanaerobacter ethanolicus*. *Int. J. Syst. Bacteriol.* **1993**, *43*, 41–51. [[CrossRef](#)]
29. Kim, I.J.; Kim, S.R.; Kim, K.H.; Bornscheuer, U.T.; Nam, K.H. Characterization and structural analysis of the endo-1,4- $\beta$ -xylanase GH11 from the hemicellulose-degrading *Thermoanaerobacterium saccharolyticum* useful for lignocellulose saccharification. *Sci. Rep.* **2023**, *13*, 17332. [[CrossRef](#)]
30. Nam, K.H. Data of serial synchrotron crystallography of xylanase GH11 from *Thermoanaerobacterium saccharolyticum*. *Data Brief* **2024**, *52*, 110055. [[CrossRef](#)] [[PubMed](#)]
31. Nam, K.H. Comparative Analysis of Room Temperature Structures Determined by Macromolecular and Serial Crystallography. *Crystals* **2024**, *14*, 276. [[CrossRef](#)]
32. Nam, K.H. pH-Induced structural changes in xylanase GH11 from *Thermoanaerobacterium saccharolyticum*. *F1000Research* **2024**, *13*, 242. [[CrossRef](#)]
33. Gu, D.H.; Eo, C.; Hwangbo, S.A.; Ha, S.C.; Kim, J.H.; Kim, H.; Lee, C.S.; Seo, I.D.; Yun, Y.D.; Lee, W.; et al. BL-11C Micro-MX: A high-flux microfocus macromolecular-crystallography beamline for micrometre-sized protein crystals at Pohang Light Source II. *J. Synchrotron Radiat.* **2021**, *28*, 1210–1215. [[CrossRef](#)] [[PubMed](#)]
34. Otwinowski, Z.; Minor, W. Processing of X-ray diffraction data collected in oscillation mode. *Methods Enzymol.* **1997**, *276*, 307–326. [[CrossRef](#)]
35. Vagin, A.; Teplyakov, A. Molecular replacement with MOLREP. *Acta Crystallogr. D Biol. Crystallogr.* **2010**, *66*, 22–25. [[CrossRef](#)] [[PubMed](#)]
36. Casañal, A.; Lohkamp, B.; Emsley, P. Current developments in Coot for macromolecular model building of Electron Cryo-microscopy and Crystallographic Data. *Protein Sci.* **2020**, *29*, 1055–1064. [[CrossRef](#)]
37. Liebschner, D.; Afonine, P.V.; Baker, M.L.; Bunkoczi, G.; Chen, V.B.; Croll, T.I.; Hintze, B.; Hung, L.W.; Jain, S.; McCoy, A.J.; et al. Macromolecular structure determination using X-rays, neutrons and electrons: Recent developments in Phenix. *Acta Crystallogr. D Struct. Biol.* **2019**, *75*, 861–877. [[CrossRef](#)] [[PubMed](#)]
38. Williams, C.J.; Headd, J.J.; Moriarty, N.W.; Prisant, M.G.; Videau, L.L.; Deis, L.N.; Verma, V.; Keedy, D.A.; Hintze, B.J.; Chen, V.B.; et al. MolProbity: More and better reference data for improved all-atom structure validation. *Protein Sci.* **2018**, *27*, 293–315. [[CrossRef](#)] [[PubMed](#)]
39. Camacho, C.; Coulouris, G.; Avagyan, V.; Ma, N.; Papadopoulos, J.; Bealer, K.; Madden, T.L. BLAST+: Architecture and applications. *BMC Bioinform.* **2009**, *10*, 421. [[CrossRef](#)] [[PubMed](#)]
40. Larkin, M.A.; Blackshields, G.; Brown, N.P.; Chenna, R.; McGettigan, P.A.; McWilliam, H.; Valentin, F.; Wallace, I.M.; Wilm, A.; Lopez, R.; et al. Clustal W and Clustal X version 2.0. *Bioinformatics* **2007**, *23*, 2947–2948. [[CrossRef](#)]
41. Gouet, P.; Courcelle, E.; Stuart, D.I.; Metz, F. ESPript: Analysis of multiple sequence alignments in PostScript. *Bioinformatics* **1999**, *15*, 305–308. [[CrossRef](#)]

**Disclaimer/Publisher’s Note:** The statements, opinions and data contained in all publications are solely those of the individual author(s) and contributor(s) and not of MDPI and/or the editor(s). MDPI and/or the editor(s) disclaim responsibility for any injury to people or property resulting from any ideas, methods, instructions or products referred to in the content.